

# Development of an experimental set-up for low-temperature spectroscopic studies of matrix-isolated molecules and molecular ices using synchrotron radiation

Param Jeet Singh,<sup>a\*</sup> K. Sundararajan,<sup>b,c</sup> Aparna Shastri,<sup>a,c</sup> Vijay Kumar,<sup>d</sup> Asim Kumar Das,<sup>a</sup> P. K. Kush<sup>e</sup> and B. N. Raja Sekhar<sup>a,c</sup>

Received 17 April 2018

Accepted 20 July 2018

Edited by S. Svensson, Uppsala University, Sweden

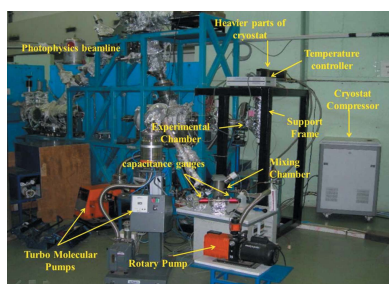
**Keywords:** synchrotron radiation; matrix isolation; low temperature; VUV spectroscopy; molecular ices; FTIR.

<sup>a</sup>Atomic and Molecular Physics Division, BARC, Mumbai, India, <sup>b</sup>Materials Chemistry Division, MC&MFCG, IGCAR, Kalpakkam, India, <sup>c</sup>Homi Bhabha National Institute, Mumbai, India, <sup>d</sup>Laser Biomedical Application Section, RRCAT, Indore, India, and <sup>e</sup>Cryo-engineering and Cryo-module Development Section, RRCAT, Indore, India. \*Correspondence e-mail: singhp@barc.gov.in

An experimental set-up for studying photophysics and photochemistry of molecules in an inert gas medium (matrix-isolated) and in the ice phase at low temperatures has been developed and commissioned at the Photophysics beamline, Indus-1 synchrotron radiation source. This end-station uses an in-house-developed closed-cycle cryostat for achieving cryo-temperatures ( $\sim 10$  K). Synchrotron radiation from the Photophysics beamline is used as the source of UV–VUV photons and the system is equipped with a Fourier transform infrared spectrometer for characterization of the molecular species formed at low temperature. Various individual components of the end-station like closed-cycle cryostat, experimental chamber, gas mixing and deposition systems are tested to ascertain that the desired performance criteria are satisfied. The performance of the composite system after integration with the Photophysics beamline is evaluated by recording IR and UV–VUV photo-absorption spectra of sulfur dioxide at low temperatures (10 K), both in the ice phase as well as isolated in argon matrices. Results obtained are in good agreement with earlier literature, thus validating the satisfactory performance of the system. As an off-shoot of the study, the VUV absorption spectrum of matrix-isolated  $\text{SO}_2$  in argon matrix up to 10.2 eV is reported here for the first time. This experimental end-station will provide new opportunities to study photon-induced reactions in molecules of environmental, astrochemical and industrial importance. Details of the design, development and initial experimental results obtained are presented.

## 1. Introduction

Over the past few decades, low-temperature techniques have been used by several groups to carry out photophysics and photochemistry of matrix-isolated molecules and molecular ices (Barnes, 1984; Baskir *et al.*, 2009; Bondybey *et al.*, 1996; Chen *et al.*, 2014; Cruz-Diaz *et al.*, 2014a; Dunkin, 1998; Gerber, 2004; Jacox, 2002; Jheeta *et al.*, 2013; Klaeboe & Nielsen, 1992; Ochsner *et al.*, 1998; Perutz, 1985; Pfeilsticker *et al.*, 2001; Tasumi & Nakata, 1985; Viswanathan *et al.*, 2006; Wu *et al.*, 2009, 2012; Young, 2014). Matrix-isolation spectroscopy (MIS) is a well established technique in which the sample of interest (guest) is mixed with a large excess of inert gas (host) and deposited on a substrate at low temperature ( $\sim 10$  K) (Moss *et al.*, 2004; Barnes, 1984; Baskir *et al.*, 2009; Bondybey *et al.*, 1996; Dunkin, 1998; Gerber, 2004; Jacox, 2002; Klaeboe & Nielsen, 1992; Lu *et al.*, 2006; Norman & Porter, 1954;



© 2018 International Union of Crystallography

Perutz, 1985; Pfeilsticker *et al.*, 2001; Sneep *et al.*, 2006; Tasumi & Nakata, 1985; Tiedje *et al.*, 2001; Viswanathan *et al.*, 2006; Whittle *et al.*, 1954; Wu *et al.*, 2009). Highly reactive molecules or radicals with very short lifetimes are thus stabilized in inert matrices and spectroscopic studies of such exotic species can be performed conveniently using this technique. The trapped species are studied with a variety of characterization techniques like FTIR (Fourier transform infrared), Raman, electron spin resonance, UV–visible or vacuum ultraviolet (VUV) absorption spectroscopy, fluorescence, electron energy-loss spectroscopy, *etc.* (Almeida *et al.*, 2014; Baskir *et al.*, 2009; Bondybey *et al.*, 1996; Cruz-Diaz *et al.*, 2014a,b; Gerber, 2004; Jacox, 2002; Monninger *et al.*, 2002; Pfeilsticker *et al.*, 2001; Sneep *et al.*, 2006; Tiedje *et al.*, 2001; Viswanathan *et al.*, 2006; Young, 2014). Characteristic advantages like transparency of rare gas matrices, lack of appreciable diffusion, weak guest–host interactions, restricted rotational structure and elimination of hot bands have fuelled the use of the MIS technique (Moss *et al.*, 2004; Baskir *et al.*, 2009; Gerber, 2004; Viswanathan *et al.*, 2006). The MIS technique finds diverse applications in atmospheric chemistry (Viswanathan *et al.*, 2006), study of weak hydrogen-bonding interactions (Jiang *et al.*, 2017), charge transfer and van der Waals complexes (Lu *et al.*, 2006), spectroscopy of transient species (Baskir *et al.*, 2009), conformational studies in molecules (Bondybey *et al.*, 1996) and investigation of reaction intermediates and mechanisms (Jacox, 2002). MIS also offers possibilities to study changes in electronic and vibrational energies in rare-gas matrices, identification of the valence/Rydberg nature of molecular excited states *via* shifts in electronic transition energies in the gas phase and matrix-isolation (MI) phase (Robin, 1976), simplification of the spectrum by eliminating hot bands and freezing the rotational structure. Synchrotron radiation (SR), with its high intensity and tunability, is an ideal source for studying photoabsorption and UV/VUV photolysis of matrix-isolated molecules and molecular ices (Almeida *et al.*, 2014; Dickgießer & Schwentner, 2000; Holtom *et al.*, 2006; Lu *et al.*, 2005; Parnis *et al.*, 2009; Mason *et al.*, 2006; Monninger *et al.*, 2002; Young, 2014). Despite the vast range of scientific issues that could be investigated by SR-based VUV spectroscopy of molecules in the MI and ice phase (Mason *et al.*, 2006; Monninger *et al.*, 2002; Nobre *et al.*, 2008; Young, 2014), there are few dedicated experimental facilities worldwide catering to this area of research. Amongst the currently operational synchrotron facilities catering to gas-phase molecular spectroscopy, a mention must be made of the VUV beamlines at Indus-1, India (Singh *et al.*, 2011), Aarhus, Denmark (Jones *et al.*, 2017), Swiss Light Source (Bodi *et al.*, 2012), Elettra, Italy (Strählman *et al.*, 2016), NSRRC, Taiwan (Lu *et al.*, 2005), Canadian Light Source (Śmiałek *et al.*, 2017), Chemical Dynamics beamline, Berkeley, USA (Stein *et al.*, 2017) and Soleil, France (Oliveira *et al.*, 2016). In particular, at ASTRID, Aarhus and NSRRC, low-temperature facilities coupled with VUV beamlines have been used to study a variety of molecules of astrophysical interest in ice and MI phases using VUV SR (Sivaraman *et al.*, 2014; Wu *et al.*, 2010). More recently, the undulator-based DESIRS beamline at Soleil, with its unique

capability of ultrahigh resolution and high brilliance, offers a state-of-the-art facility for VUV spectroscopy of dilute species like radicals and reaction intermediates in the gas phase (Hartweg *et al.*, 2017; Nahon *et al.*, 2012), which are complementary to the study of such species in the matrix-isolated phase.

In order to exploit the dual advantages of the MI technique and SR as a source and considering the current scientific interest in studies of exotic/unstable species, a low-temperature set-up has been designed, developed and installed at the Photophysics beamline, Indus-1, Raja Ramanna Centre for Advance Technology (RRCAT), Indore, India (Meenakshi Raja Rao *et al.*, 2001). Using a gas-phase experimental station coupled to the Photophysics beamline, UV–VUV photoabsorption studies of several polyatomic molecules (Mandal *et al.*, 2014; Shastri *et al.*, 2017; Singh *et al.*, 2013) have been performed over the past few years. For the low-temperature experiments, the monochromatized SR beam ( $\sim 3.5$ – $11.8$  eV) with a flux of  $\sim 10^9$  photon  $\text{s}^{-1}$  ( $0.1\%$  bandwidth) $^{-1}$  is used for photolysis of the trapped molecules and ices and/or recording their electronic absorption spectra. The set-up is equipped with an FTIR spectrometer useful for identification/characterization of the molecular ices or matrix-isolated species *via* observation of their vibrational spectra. Details of the design, development and performance evaluation of the experimental set-up are discussed. Further, the IR and UV–VUV absorption spectra of sulfur dioxide (SO<sub>2</sub>) isolated in argon matrix and its UV–VUV spectrum in the ice phase recorded after integrating the system with the synchrotron beamline are presented.

## 2. Description of the experimental set-up

The MIS set-up consists of a closed-cycle helium cryostat, a chiller unit, an experimental chamber, sample-mixing chamber, vacuum system, temperature sensor, and interconnecting gas lines for preparation of sample mixtures with inert gases. Schematic diagrams of the cryostat and experimental chamber and 3-D models of experimental and mixing chambers are shown in Figs. 1(a)–1(d). A view of the MIS set-up after integration with the Photophysics beamline is shown in Fig. 2.

Rare-gas matrices are generally prepared by depositing gaseous flux onto a cold window kept in a cryostat at low temperatures ( $\sim 10$  K). A closed-cycle cryostat (*cf.* Fig. 1a) developed in-house at RRCAT is used in the present experimental set-up (Dunkin, 1998; Kush *et al.*, 2004, 2010). The cryostat is based on the Gifford–McMahon principle in which cooling is achieved by isentropic expansion of helium gas in a closed loop. It is a cascaded two-stage system with cooling capacity of 8 W at 50 K and 1.5 W at 10 K (Kush *et al.*, 2004, 2010). The main components of the cryostat are a helium compressor, cold head, chiller unit and temperature-controller sensors. The cryostat is mounted on the support frame structure with ball bearings in such a way that the heavier parts are mounted on the top as shown in Fig. 2. A sample holder made of oxygen-free high-conductivity copper for holding a 1 inch-

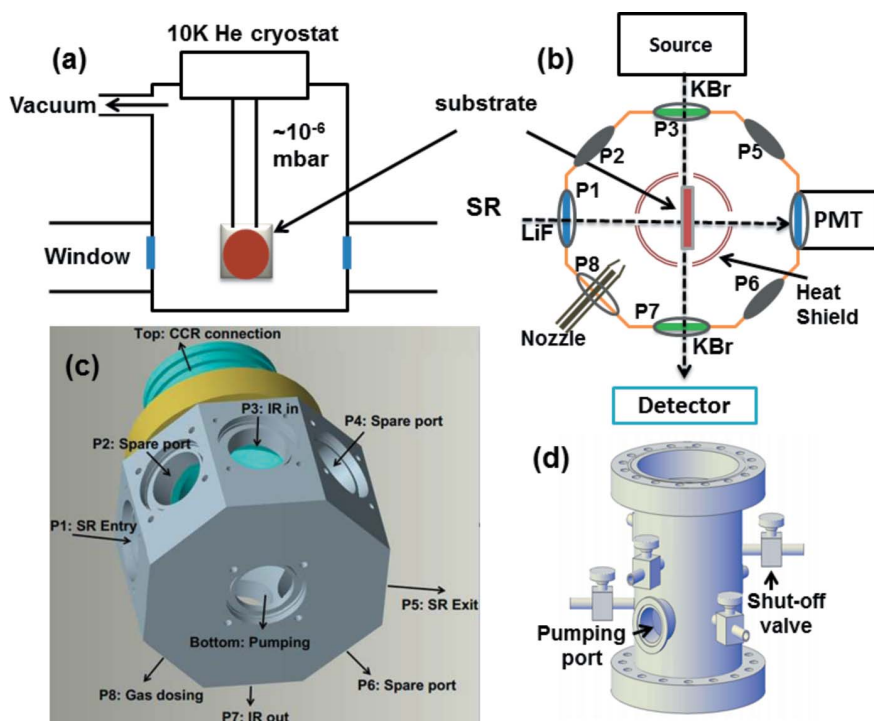


**Figure 1**  
Schematic diagrams of (a) the vertical cross section of the cryostat and (b) the horizontal cross section of the experimental chamber. 3-D models of (c) the experimental chamber and (d) the mixing chamber. P1–P8: ports of the octagonal chamber. PMT: photomultiplier tube.

diameter substrate is connected to the cryostat. The cryo-tip has a heat shield around the cold head with four openings at 90° (*cf.* Fig. 1*b*).

The experimental chamber is an octagonal stainless steel chamber with eight ports (P1 to P8) as shown in Figs. 1*(b)* and 1*(c)*. Two additional ports (P9 and P10) are provided for connecting the chamber to the cryostat and for pumping. Ports P1 and P5 are used for entry and exit of the SR. Port P2, at 45° to the SR entry, is used for connecting the nozzle for sample

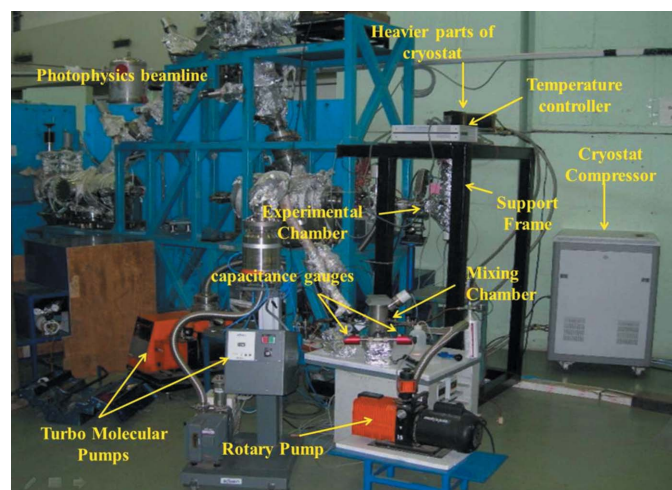


**Figure 2**  
Photograph of the MIS set-up after integration with the Photophysics beamline.

deposition. Ports P3 and P7 are provided for coupling of diagnostic equipment like a FTIR spectrometer. The remaining ports (P4, P6 and P8) are available for sample-thickness measurements and/or for future up-gradation of the experimental end-station by incorporating additional characterization techniques. The cold tip assembly is inserted into the experimental chamber through an O-ring-based rotary feed-through (P9) which enables 360° rotation under vacuum. The inner diameter of ports P1–P8 is 35 mm and port P10 is connected to the cryostat *via* an O-ring-based vulcanized seal.

The mixing chamber is a stainless steel cylindrical container with CF 63 connections on both ends to connect SS blanks and with six quarter-inch tube connectors (*cf.* Fig. 1*d*) which are used for different functions like pressure measurement, inlet of gases/gas mixtures and connection to the experimental chamber for deposition. Both the chambers are evacuated to a base pressure of  $\sim 1 \times 10^{-6}$  mbar using turbo-molecular pumps (Model TurboPAC-140, Pfeiffer Vacuum) and pressure is measured using cold cathode ionization gauges (Model PKR251, Pfeiffer Vacuum). The sample gas of interest is mixed with high-purity argon (99.995%) in the mixing chamber at appropriate manometric ratios, typically 1:1000 to 1:100, using a set of two capacitance manometers (CMR 361 and CMR 363, Pfeiffer Vacuum). The measurement ranges of the two gauges are 10–0.001 mbar (reading accuracy 0.5%) and 5000–0.5 mbar (reading accuracy 0.15%), respectively. A calibrated needle valve (Model No. EVN 116, Pfeiffer Vacuum) connected to a 200  $\mu\text{m}$  deposition nozzle located at a distance of 10 mm from the heat shield is used to deposit the gas mixture. During deposition the sample holder assembly (cold tip) is rotated by 45° so as to face the nozzle (*cf.* Fig. 1*b*). Connectors used are of stainless steel, quarter-inch ferrule type and all-metal. Swagelok shut-off valves are used for isolation of the chamber from the gauges and sample inlets.

### 3. Off-line testing of subsystems and assembly

The various subsystems such as experimental chamber, mixing chamber, vacuum systems, gas lines and nozzle, leak valves, temperature sensor, capacitance manometers, *etc.* are tested individually and assembled. These include mechanical stability tests of the sample holder, temperature calibration and measurement as well as leak testing and vacuum testing of the system. Vibration measurements are carried out to evaluate the effect of vibrations produced by the compressor on the sample holder. For the vibration measurements, light from a 0.5 mW diode laser is made to fall at the centre of a glass

substrate mounted in the sample holder and the image of the reflected laser spot is captured at  $90^\circ$  to the incident direction using an analog CCD camera having a resolution of  $10\ \mu\text{m}$ . Change in the centroid position of the light spot gives a measure of the amplitude of the vibrations and the corresponding change in position with reference to the average position. The maximum mechanical fluctuations are found to be within  $\pm 250\ \mu\text{m}$  ( $\pm 60\ \mu\text{m}$ ) in the horizontal (vertical) direction, which are much smaller than the typical defocused spot size  $8\ \text{mm}$  (H)  $\times$   $6\ \text{mm}$  (V) of the SR beam used in the photoabsorption experiments and are hence well within acceptable limits.

The temperature of the sample in the cryostat is monitored with a calibrated silicon sensor (Model DT470, Lake Shore) placed at the bottom of the sample holder and read out using a temperature controller (Model No.Ls-325, Lake Shore). A resistive heating arrangement using a kapton-coated nichrome wire is provided to anneal the sample from 10 K to 300 K *in situ*. The temperature variation of the sample holder measured during cooling and heating cycles is shown in Fig. 3. The typical time taken to reach the final temperature of 10 K is  $\sim 2\ \text{h}$ . The sudden sharp decrease in temperature below  $\sim 30\ \text{K}$  may be attributed to faster adsorption of residual gases effectively increasing the rate of cooling. Fig. 3 also shows the behaviour of the temperature of the sample holder after the cryostat is switched off. To set a desired temperature in the range 10–300 K the sample holder is heated in a controlled manner which can be achieved with a relative temperature stability of  $\pm 0.5\ \text{K}$  for a set value.

The system is leak tested with a He mass spectrometric leak detector and no leak is detected within  $2 \times 10^{-9}\ \text{mbar l s}^{-1}$ . A base pressure of  $1 \times 10^{-6}\ \text{mbar}$  is achieved in the cryostat at room temperature which further improves to  $3 \times 10^{-7}\ \text{mbar}$  at 10 K due to cryopumping.

#### 4. Integration of the end-station with the beamline

After successful offline testing of the subsystems, the assembled end-station is integrated with the Photophysics beamline. The Photophysics beamline operates in the wavelength region 1050–3500 Å (3.5–11.8 eV) and SR is dispersed by the 1 m Seya-Namioka monochromator of the beamline with a spectral resolution of  $\sim 6\ \text{meV}$  at 6 eV and  $\sim 11\ \text{meV}$  at 11 eV. Monochromatized radiation passes through the experimental chamber and the transmission profile is recorded using a UV-visible photomultiplier tube coupled with a sodium salicylate-coated quartz window, which acts as a scintillator to convert the VUV radiation into visible radiation. An LiF-windowed gate valve (transmission cut-off at 11.8 eV) is used to isolate the experimental chamber from the rest of the beamline

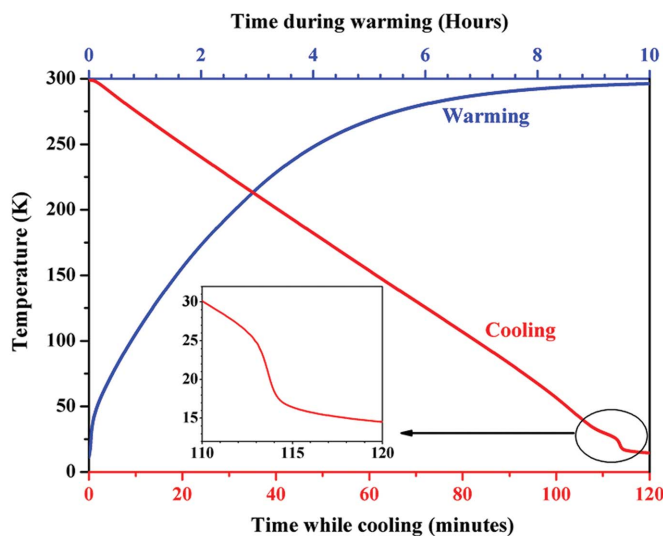


**Figure 3** Temperature profile during cooling (red) and warming cycles (blue). Time scales at the bottom and top correspond to cooling and warming cycles, respectively.

(*cf.* Fig. 4). The system is equipped with an FTIR spectrometer (IS10 and IZ10, Thermo Fischer Scientific; resolution  $0.5\ \text{cm}^{-1}$ ) placed in such a way as to facilitate *in situ* recording of FTIR spectra as shown in Fig. 4. For these measurements, IR beam from the globar source of the FTIR spectrometer is aligned to pass through the centre of the experimental chamber in a direction perpendicular to the SR beam. For wavelength calibration in the VUV region, a gas cell is connected between the beamline and the MI chamber which enables simultaneous recording of absorption spectra of Xe atomic lines and the molecule under study. A  $\text{CaF}_2$  window (transmission cut-off at 9.92 eV) mounted in the sample holder of the cryostat is used as substrate to deposit molecules of interest. The deposited samples are characterized with FTIR in the region  $900\text{--}4000\ \text{cm}^{-1}$  and UV–VUV photoabsorption studies are performed using SR in the region from 3.7 to 9.9 eV.

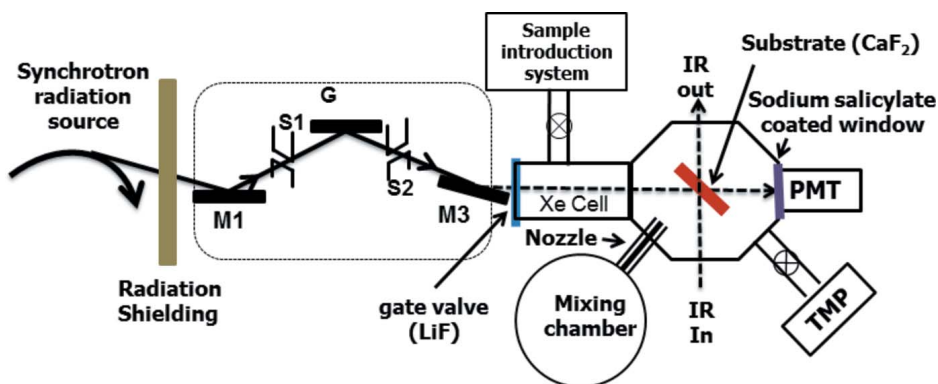


**Figure 4** Schematic of the Photophysics beamline and end-station after integration with the FTIR spectrometer. M1: toroidal gold-coated pre-mirror. G: gold-coated spherical grating. M2: gold-coated toroidal post-mirror. S1: entrance slit. S2: exit slit. The Xe cell is used for calibration of VUV wavelengths.

## 5. Photoabsorption spectroscopy of SO<sub>2</sub> in Ar matrix and the ice phase: IR and UV–VUV study

The performance of the integrated end-station is evaluated by performing IR and UV–VUV absorption studies of SO<sub>2</sub> in argon matrix as well as in the ice phase. Sulfur dioxide molecules are present as pollutants in the earth's atmosphere and also found in various extra-terrestrial objects like comets and planets (Jessup *et al.*, 2007; Li *et al.*, 2004; Loyola *et al.*, 2008; Palmer *et al.*, 2005; Singh *et al.*, 2012; Wilkinson *et al.*, 2014). Due to its important role in atmospheric chemistry, there has been a continued interest in the spectroscopy and photochemistry of this molecule. While the room-temperature electronic absorption spectrum of SO<sub>2</sub> in the gas phase has been studied quite extensively (Ahmed & Kumar, 1992; Danielache *et al.*, 2008; Hermans *et al.*, 2009; Li *et al.*, 2004; Palmer *et al.*, 2005; Singh *et al.*, 2011, 2012; Wilkinson *et al.*, 2014), several groups have reported on the low-temperature spectrum of SO<sub>2</sub> ice (Holtom *et al.*, 2006; Mason *et al.*, 2006) as well as on matrix-isolated SO<sub>2</sub> (Hirabayashi *et al.*, 2006; Ito & Hirabayashi, 2009). In view of the considerable importance of photochemistry of this molecule in atmospheric and astrochemical sciences, and the availability of IR and UV–VUV spectral data for comparison, SO<sub>2</sub> is chosen for the preliminary experiments using the low-temperature end-station.

For the matrix-isolation studies, a mixture of SO<sub>2</sub> and Ar is prepared in the ratio 1:800 in the mixing chamber using standard manometric procedures and the mixture is slowly allowed to deposit onto the cold CaF<sub>2</sub> window through a single jet nozzle. Films are prepared under different deposition conditions (total deposition: 2–50 mbar) starting with a pressure of 1000 mbar in the mixing chamber. During deposition, a constant pressure drop of  $\sim 1$  mbar min<sup>-1</sup> is maintained which approximately corresponds to a film deposition rate of  $\sim 4 \times 10^{-2}$   $\mu\text{m min}^{-1}$ . For the total deposition of 2–50 mbar, we estimate the resultant film thickness to be  $\sim 0.08$ – $2$   $\mu\text{m}$ .

The FTIR spectrum of SO<sub>2</sub> in Ar matrix deposited at 10 K is shown in Fig. 5. The film thickness is estimated to be  $\sim 1.2$   $\mu\text{m}$  corresponding to a total deposition time of 30 min. SO<sub>2</sub> is known to occupy stable and metastable sites in argon matrix which originate from the site substitution in hexagonal-close-packed and face-centred-cubic lattice of Ar crystal, respectively (Ito & Hirabayashi, 2009). The strongest features in the spectrum observed at 1355.0 cm<sup>-1</sup> and 1351.2 cm<sup>-1</sup> may be assigned to site split features arising from the  $\nu_3$  S–O asymmetric stretching mode of the SO<sub>2</sub> monomer in Ar matrix (Ito & Hirabayashi, 2009). Similarly, the bands at 1152.1 cm<sup>-1</sup> and 1147.2 cm<sup>-1</sup> with somewhat lower intensity (*cf.* Fig. 5) can be assigned to the site split features of the  $\nu_1$  symmetric stretching mode of SO<sub>2</sub> (Ito & Hirabayashi, 2009). The rest of the observed bands which are relatively weak have been attributed to various modes of SO<sub>2</sub> clusters as follows. The features observed at 1349 cm<sup>-1</sup>, 1348.1 cm<sup>-1</sup>, 1346 cm<sup>-1</sup>, 1343.4 cm<sup>-1</sup> and 1341.5 cm<sup>-1</sup> are assigned to the  $\nu_3$  mode, while a weak feature observed at 1150 cm<sup>-1</sup> is due to the  $\nu_1$  mode of SO<sub>2</sub> clusters (Ito & Hirabayashi, 2009). Two additional peaks observed at 1338.3 cm<sup>-1</sup> and 1334.5 cm<sup>-1</sup> (marked with \*) are

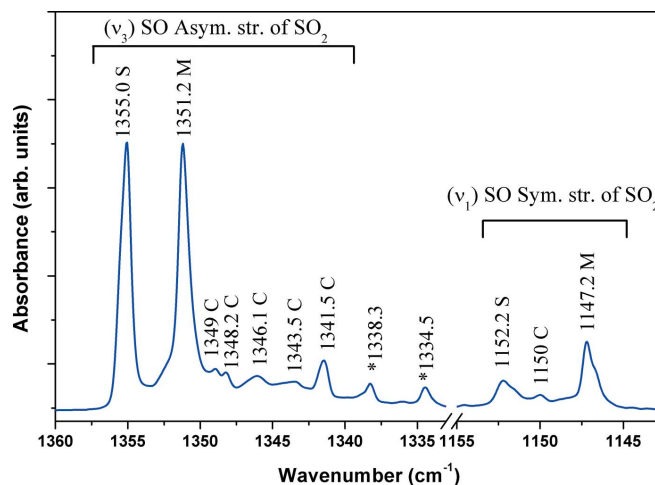


Figure 5

Infrared spectrum of SO<sub>2</sub> isolated in Ar matrix at 10 K. M: SO<sub>2</sub> monomer in metastable site. S: SO<sub>2</sub> monomer in stable site. C: peaks due to SO<sub>2</sub> clusters. \*Peak due to the <sup>34</sup>SO<sub>2</sub> monomer and SO<sub>2</sub>–H<sub>2</sub>O cluster.

tentatively assigned to the <sup>34</sup>SO<sub>2</sub> monomer in a metastable site and SO<sub>2</sub>–H<sub>2</sub>O cluster in Ar matrix, respectively (Hirabayashi *et al.*, 2006). All the spectral features observed in the IR spectrum of SO<sub>2</sub> in Ar matrix in the present work agree well with the spectra reported in the literature (Hirabayashi *et al.*, 2006; Ito & Hirabayashi, 2009), thus validating the performance of the MIS set-up.

The next case study taken up is the UV–VUV absorption spectrum of SO<sub>2</sub> in the MI and ice phases. Samples of pure SO<sub>2</sub> and SO<sub>2</sub> mixed with argon in different ratios ranging from 0.2:1000 to 5:1000 are deposited on the CaF<sub>2</sub> substrate at 10 K. The UV–VUV absorption spectrum of SO<sub>2</sub> gas (room temperature) is recorded for the purpose of comparison. Experiments are performed under different deposition conditions. To study the effects of annealing, the absorption spectrum of SO<sub>2</sub> ice after annealing and cooling back to 10 K is also recorded. The spectra of SO<sub>2</sub> recorded in the region 3.5–10 eV in gas, MI and ice phases are compared in Fig. 6. The effect of different mixing ratios (SO<sub>2</sub>:Ar) on the MI phase absorption spectra is shown in Fig. 7. The estimated film thickness from optimum deposition of 20 min for the spectra presented in Figs. 6 and 7 is  $\sim 0.8$   $\mu\text{m}$ . It should be mentioned that the absorption cross sections of the molecules in the UV–VUV regions are relatively higher than in the IR region, therefore thinner films are used for UV–VUV absorption experiments.

The gas-phase absorption spectrum of SO<sub>2</sub> comprises several electronic band systems classically designated as  $\bar{A}$ – $\bar{X}$ ,  $\bar{B}$ – $\bar{X}$ ,  $\bar{C}$ – $\bar{X}$ ,  $\bar{D}$ – $\bar{X}$ ,  $\bar{E}$ – $\bar{X}$ ,  $\bar{F}$ – $\bar{X}$  and  $\bar{G}$ – $\bar{X}$  as marked in Fig. 6(a) (Palmer *et al.*, 2005). All the observed band systems show an overall blue shift in going from the gas phase to the matrix-isolated phase, with the magnitude of the shift varying from system to system. Within each system, the individual vibrational bands also shift in the MI phase compared with the gas phase in a non-uniform manner. The small magnitude of shift observed for the electronic transitions corresponding to the  $\bar{A}$ ,  $\bar{B}$ ,  $\bar{C}$ ,  $\bar{D}$  and  $\bar{E}$  systems indicates that these are predominantly

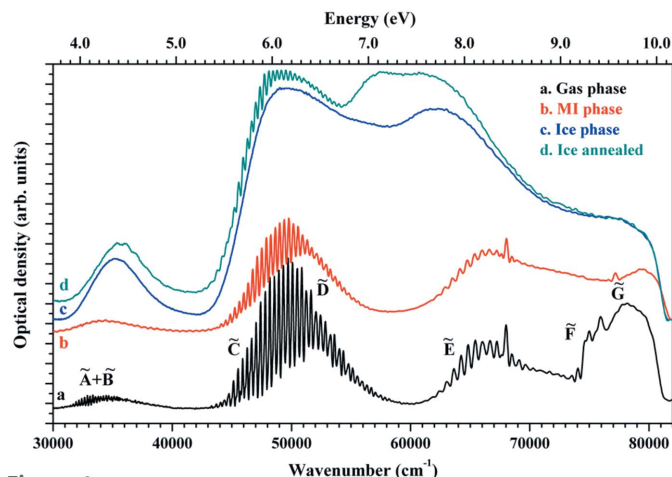


**Figure 6**  
VUV absorption spectrum of SO<sub>2</sub> recorded using SR. (a) Gas phase, (b) isolated in argon matrix at 10 K with an SO<sub>2</sub>:Ar mixing ratio of 2:1000. (c) Ice phase at 10 K. (d) After annealing up to 80 K and cooling back to 10 K. The gas phase spectrum is displaced vertically for clarity.

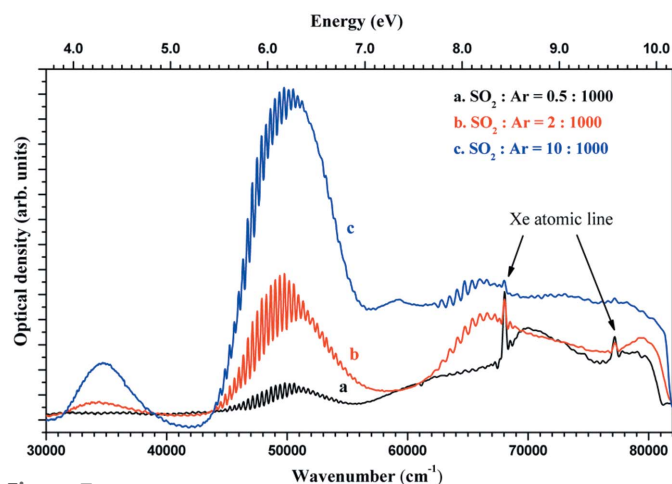


**Figure 7**  
VUV absorption spectrum of matrix-isolated SO<sub>2</sub> at 10 K using different mixing ratios of SO<sub>2</sub>:Ar: (a) 0.5:1000, (b) 2:1000, (c) 10:1000.

valence excitations (Robin, 1976). In contrast, the transitions appearing in the gas phase above 9 eV, attributed to the Rydberg series (Singh *et al.*, 2012), disappear completely in MI as well as in the ice phase. This is as expected since Rydberg states are known to be either heavily blue shifted or completely obliterated in the MI/ice phase (Lepage *et al.*, 2000; Robin, 1976).

Peak positions of bands corresponding to the  $\tilde{A} + \tilde{B}$  system [Clement's band (Herzberg, 1966)] observed in the 3.8–5.0 eV region for the gas and MI phase are shown in Table 1 along with those reported earlier (Brand & Nanes, 1973; Metropolis, 1941; Phillips *et al.*, 1969). Considering the broad nature of the bands and the measurement accuracy of  $\pm 20 \text{ cm}^{-1}$ , the present MI results are in good agreement with earlier work on SO<sub>2</sub> in krypton matrix (*cf.* Table 1), where some of these bands were tentatively assigned to the progression  $A(\nu'_1, \nu'_2, 0) \leftarrow X(0, 0, 0)$  (Phillips *et al.*, 1969). It may be noted that, in the MI phase at low concentration of SO<sub>2</sub>, this band is observed to

**Table 1**  
Vibronic bands (in  $\text{cm}^{-1}$ ) observed in the  $\tilde{A} + \tilde{B}$  system of SO<sub>2</sub>.

Gas phase			MI phase	
Present work	Brand & Nanes (1973)	Metropolis (1941)	Present work	Phillips <i>et al.</i> (1969)
31459	31437	–	–	–
31705	31717	–	31629	–
31932	31936	–	31837	–
32179	32181	32198	32103	32180
32405	32394	32377	32311	32410
32652	32619	32607	32576	32685
32879	32866	32850	32823	32895
33107	33089	33080	33088	33110
33334	33318	33313	33315	33320
33561	–	33547	33543	33540
33789	–	33760	33751	33780
33997	–	33960	33990	33970
34224	–	34240	34201	34240
34451	–	34396	34423	34420
34660	–	34620	34683	34645
34901	–	34785	34941	34825
35115	–	35068	–	35020
35361	–	35236	35394	35270
35600	–	35556	–	35530

be weak with overriding vibrational structure while, at higher concentrations and in the ice phase, it appears as a broad hump. After annealing the SO<sub>2</sub> ice up to 80 K and cooling back to 10 K, a few weak structures with a spacing of  $\sim 750\text{--}870 \text{ cm}^{-1}$  are seen which may be attributed to the  $\nu'_1$  mode (Holtom *et al.*, 2006).

In the energy region 5.2–7.2 eV, the  $\tilde{C} + \tilde{D}$  system exhibits a rich band structure in the gas phase (Golomb *et al.*, 1962; Palmer *et al.*, 2005). Going from the gas phase to the MI phase, prominent vibrational structure is retained with a separation of  $\sim 380 \text{ cm}^{-1}$  which may be tentatively assigned to the  $\nu'_2$  mode. In the ice phase at 10 K, this band is devoid of vibrational structure but upon annealing to 80 K and cooling back to 10 K some structure begins to appear (*cf.* Fig. 6). This has been attributed to formation of an amorphous structure at 10 K which transforms into a more stable crystalline structure upon annealing (Holtom *et al.*, 2006). Weaker features seen in the gas-phase spectrum may be due to hot bands as evident from their disappearance in the low-temperature (MI and ice phase) spectra.

The observed peaks in the gas- and MI-phase spectra in the energy region 7.4–9.0 eV are listed in Table 2. To the best of our knowledge, the VUV absorption spectrum of matrix-isolated SO<sub>2</sub> in argon matrix up to 10.2 eV is reported here for the first time. As can be seen from the table, there is a small shift in the vibronic bands between the MI and gas phase which confirms the predominantly valence nature of the electronic states involved as proposed in earlier gas-phase work (Singh *et al.*, 2012). In the ice phase, this band system appears as a broad structureless hump in which the peaks at 7.8 and 8.4 eV reported by Holtom *et al.* (2006) are barely distinguishable. Upon annealing up to 80 K and cooling back to 10 K, a new feature is observed at  $\sim 7.2 \text{ eV}$ . This has been explained by Holtom *et al.* (2006) as arising due to Davydov splitting in the crystalline phase of SO<sub>2</sub>. Disappearance of

**Table 2**

 Vibronic bands (in  $\text{cm}^{-1}$ ) observed in  $\tilde{E}-\tilde{X}$  systems of  $\text{SO}_2$ .

Gas phase	MI phase
61844	61787
62394	62317
63018	62924
63605	63511
64231	64136
64818	64761
65424	65387
66031	65993
66656	66618
67262	67243
67660	67622
68512	68493
–	68891
69118	69110
69629	69573
70293	70263

the vibrational structure on condensation at 10 K suggests quenching of the vibrational modes in the ice phase.

## 6. Conclusions

An experimental end-station for low-temperature spectroscopy of molecules in the ice phase and matrix isolation phase has been designed, developed and commissioned at the Photophysics beamline, Indus-1. This end-station exploits the dual advantages of low-temperature spectroscopy of molecules and synchrotron radiation as a light source. Testing of various individual components like closed-cycle cryostat, experimental chamber, gas mixing and deposition system are carried out to confirm their satisfactory performance. The mechanical and temperature stabilities of the cryostat are found to be within acceptable limits. Performance evaluation of the composite experimental end-station after integrating with the beamline is carried out by recording the IR and UV–VUV spectra of  $\text{SO}_2$  at low temperature (10 K), using an FTIR spectrometer and synchrotron radiation from the Photophysics beamline, respectively. The observed IR and UV–VUV absorption spectra of  $\text{SO}_2$  in argon matrices and the ice phase are in excellent agreement with the reported literature wherever available. These results demonstrate the satisfactory performance of the end-station.

It is pertinent here to make a comparison of this system with similar facilities around the world. To the best of our knowledge the only other SR facilities available currently for VUV

studies of molecules in the ice and MI phase are at Aarhus, Denmark, and NSRRC, Taiwan. The salient features of these facilities are compared with the present setup in Table 3. The main difference in these facilities as compared with the present setup is that a better base pressure of  $\leq 10^{-8}$  mbar has been achieved. Another aspect is that in the Aarhus setup the thickness of the deposited ice films are measured using a laser-based interference method, while in the present case we have estimated the thickness indirectly, knowing the deposition rate and total time for deposition.

The capability of the present system can be extended in the future by upgrading the experimental chamber to an all-metal UHV system with a facility for measuring thickness using a laser-based interference method. In all other respects, we believe that the performance of the present system is comparable with that of the other existing facilities worldwide. The set-up will be useful for a variety of studies exploiting the unique combination of UV–VUV (SR) and FTIR spectroscopy, and is expected to open up several new avenues of research in the areas of photon-induced processes and chemical reactions in molecules.

## Acknowledgements

We thank Dr N. K. Sahoo, Dr K. Sankaran and Dr S. N. Jha for their support and interest in this work. We also thank Dr D. Bhattacharyya for useful discussions and encouragement. The role of Dr B. N. Jagatap and Dr K. S. Viswanathan in initiating this work is also acknowledged.

## References

- Ahmed, S. M. & Kumar, V. (1992). *J. Quant. Spectrosc. Radiat. Transfer*, **47**, 359–373.
- Almeida, G. C., Pilling, S., Andrade, D. P. P., Castro, N. L. S., Mendoza, E., Boechat-Roberty, H. M. & Rocco, M. L. M. (2014). *J. Phys. Chem. C*, **118**, 6193–6200.
- Barnes, A. J. (1984). *J. Mol. Struct.* **113**, 161–174.
- Baskir, E. G., Misocho, E. Y. & Nefedov, O. M. (2009). *Russ. Chem. Rev.* **78**, 683–715.
- Bodi, A., Hemberger, P., Gerber, T. & Sztáray, B. (2012). *Rev. Sci. Instrum.* **83**, 083105.
- Bondybey, V. E., Smith, A. M. & Agreiter, J. (1996). *Chem. Rev.* **96**, 2113–2134.
- Brand, J. C. D. & Nanes, R. (1973). *J. Mol. Spectrosc.* **46**, 194–199.
- Chen, H.-F., Liu, M.-C., Chen, S.-C., Huang, T.-P. & Wu, Y.-J. (2015). *Astrophys. J.* **804**, 36.
- Chen, Y.-J., Chuang, K.-J., Muñoz Caro, G. M., Nuevo, M., Chu, C.-C., Yih, T.-S., Ip, W.-H. & Wu, C.-Y. R. (2014). *Astrophys. J.* **781**, 15.

**Table 3**

Comparison of the present end-station with similar facilities at synchrotrons around the world.

Parameter	Aarhus, Denmark (Dawes <i>et al.</i> , 2007)	NSRRC, Taiwan (Chen <i>et al.</i> , 2015)	Indus-1, India
Vacuum in chamber	$10^{-8}$ – $10^{-10}$ mbar	$\sim 1 \times 10^{-8}$ mbar	$1 \times 10^{-6}$ mbar
Cryostat type, make	Continuous flow, AS Scientific	Closed cycle, Janis RDK-415	Closed cycle, built in-house
Lowest temperature achieved	15 K	10 K	10 K
Film thickness measurement	Using laser beam interference	Indirect estimation	Indirect estimation
Beamline type, energy range, resolving power	Bending magnet based, $\sim 3.5$ – $12.4$ eV, $> 1000$	Undulator based, 5–100 eV, $\sim 10^5$	Bending magnet based, 4–11.8 eV, $\sim 2000$
FTIR spectrometer	Range Resolution	500–4000 $\text{cm}^{-1}$ 0.5 $\text{cm}^{-1}$	500–4000 $\text{cm}^{-1}$ 0.5 $\text{cm}^{-1}$

- Cruz-Diaz, G. A., Muñoz Caro, G. M., Chen, Y.-J. & Yih, T.-S. (2014a). *Astron. Astrophys.* **562**, A120.
- Cruz-Diaz, G. A., Muñoz Caro, G. M., Chen, Y.-J. & Yih, T.-S. (2014b). *arXiv:1405.7797*.
- Danielache, S. O., Eskebjerg, C., Johnson, M. S., Ueno, Y. & Yoshida, N. (2008). *J. Geophys. Res.* **113**, D17314.
- Dawes, A., Mukerji, R. J., Davis, M. P., Holtom, P. D., Webb, S. M., Sivaraman, B., Hoffmann, S. V., Shaw, D. A. & Mason, N. J. (2007). *J. Chem. Phys.* **126**, 244711.
- Dickgießer, M. & Schwentner, N. (2000). *Nucl. Instrum. Methods Phys. Res. B*, **168**, 252–267.
- Dunkin, I. R. (1998). *Matrix-Isolation Techniques A Practical Approach*. Oxford University Press.
- Gerber, R. B. (2004). *Annu. Rev. Phys. Chem.* **55**, 55–78.
- Golomb, D. K., Watanabe, K. & Marmo, F. F. (1962). *J. Chem. Phys.* **36**, 958–960.
- Hartweg, S., Yoder, B. L., Garcia, G. A., Nahon, L. & Signorell, R. (2017). *Phys. Rev. Lett.* **118**, 103402.
- Hermans, C. A. C., Vandaele, A. C. & Fally, S. (2009). *J. Quant. Spectrosc. Radiat. Transfer*, **110**, 756–765.
- Herzberg, G. (1966). *Molecular Spectra and Molecular Structure III*. New York: Van Nostrand Reinhold.
- Hirabayashi, S., Ito, F. & Yamada, K. M. T. (2006). *J. Chem. Phys.* **125**, 034508.
- Holtom, P. D., Dawes, A., Mukerji, R. J., Davis, M. P., Webb, S. M., Hoffmann, S. V. & Mason, N. J. (2006). *Phys. Chem. Chem. Phys.* **8**, 714–718.
- Ito, F. & Hirabayashi, S. (2009). *Chem. Phys.* **358**, 209–218.
- Jacox, M. E. (2002). *Chem. Soc. Rev.* **31**, 108–115.
- Jessup, K. L. J. R., Spencer, J. & Yelle, R. (2007). *Icarus*, **192**, 24–40.
- Jheeta, S., Domaracka, A., Ptasinska, S., Sivaraman, B. & Mason, N. J. (2013). *Chem. Phys. Lett.* **556**, 359–364.
- Jiang, X., Liu, S., Tsona, N. T., Tang, S., Ding, L., Zhao, H. & Du, L. (2017). *RSC Adv.* **7**, 2503–2512.
- Jones, D. B., Limão-Vieira, P., Mendes, M., Jones, N. C., Hoffmann, S. V., da Costa, R. F., Varela, M. T., do, N., Bettega, M. H. F., Blanco, F., García, G., Ingólfsson, O., Lima, M. A. P. & Brunger, M. J. (2017). *J. Chem. Phys.* **146**, 184303.
- Klaeboe, P. & Nielsen, C. J. (1992). *Analyst*, **117**, 335–341.
- Kush, P. K., Doohan, R. S., Sharma, R. C. & Gilankar, S. G. (2010). *RRCAT Newsl.* **23**, 26–29.
- Kush, P. K., Sharma, R. C., Doohan, R. S., Sagar, A. K., Choudhary, L. C. & Ansari, M. S. (2004). *Ind. J. Cryogen.* **29**, 69–72.
- Lepage, M. M., Michaud, M. & Sanche, L. (2000). *J. Chem. Phys.* **112**, 6707–6715.
- Li, W. Z., Huang, M. B. & Chen, B. Z. (2004). *J. Chem. Phys.* **120**, 4677–4682.
- Loyola, D., van Geffen, J., Valks, P., Erbetseder, T., Van Roozendaal, M., Thomas, W., Zimmer, W. & Wißkirchen, K. (2008). *Adv. Geosci.* **14**, 35–40.
- Lu, C., Song, G. & Lin, J. (2006). *TrAC Trends Anal. Chem.* **25**, 985–995.
- Lu, H., Chen, H., Cheng, B., Kuo, Y. & Ogilvie, J. F. (2005). *J. Phys. B At. Mol. Opt. Phys.* **38**, 3693–3704.
- Mandal, A., Singh, P. J., Shastri, A. & Jagatap, B. N. (2014). *J. Chem. Phys.* **140**, 194312.
- Mason, N. J., Dawes, A., Holtom, P. D., Mukerji, R. J., Davis, M. P., Sivaraman, B., Kaiser, R. I., Hoffmann, S. V. & Shaw, D. A. (2006). *Faraday Discuss.* **133**, 311–329.
- Meenakshi Raja Rao, P., Das, N. C., Raja Sekhar, B. N., Padmanabhan, S., Shastri, A., Bhattacharya, S. S. & Roy, A. P. (2001). *Nucl. Instrum. Methods Phys. Res. A*, **467–468**, 613–616.
- Metropolis, N. (1941). *Phys. Rev.* **60**, 295–301.
- Monninger, G., Förderer, M., Gürtler, P., Kalhofer, S., Petersen, S., Nemes, L., Szalay, P. G. & Krätschmer, W. (2002). *J. Phys. Chem. A*, **106**, 5779–5788.
- Moss, R. A., Platz, M. S. & Jones, M. Jr (2004). Editors. *Reactive Intermediate Chemistry*. Hoboken: Wiley-Interscience.
- Nahon, L., de Oliveira, N., Garcia, G. A., Gil, J.-F., Pilette, B., Marcouillé, O., Lagarde, B. & Polack, F. (2012). *J. Synchrotron Rad.* **19**, 508–520.
- Nobre, M., Fernandes, A., Ferreira da Silva, F., Antunes, R., Almeida, D., Kokhan, V., Hoffmann, S. V., Mason, N. J., Eden, S. & Limão-Vieira, P. (2008). *Phys. Chem. Chem. Phys.* **10**, 550–560.
- Norman, I. & Porter, G. (1954). *Nature (London)*, **174**, 508–509.
- Ochsner, D. W., Ball, D. W. & Kafafi, Z. H. (1998). *A Bibliography of Matrix Isolation Spectroscopy: 1985–1997*. Washington: Naval Research Laboratory.
- Oliveira, N. de, Joyeux, D., Roudjane, M., Gil, J.-F., Pilette, B., Archer, L., Ito, K. & Nahon, L. (2016). *J. Synchrotron Rad.* **23**, 887–900.
- Palmer, M. H., Shaw, D. A. & Guest, M. F. (2005). *Mol. Phys.* **103**, 1183–1200.
- Parnis, J. M., King, K. A. & Thompson, M. G. (2009). *J. Mass Spectrom.* **44**, 652–661.
- Perutz, R. N. (1985). *Chem. Rev.* **85**, 77–96.
- Pfeilsticker, K., Bösch, H., Camy-Peyret, C., Fitzenberger, R., Harder, H. & Osterkamp, H. (2001). *Geophys. Res. Lett.* **28**, 4595–4598.
- Phillips, L. F. J. J., Smith, J. J. & Meyer, B. (1969). *J. Mol. Spectrosc.* **29**, 230–243.
- Robin, M. B. (1976). *Higher Excited States of Polyatomic Molecules*, Volume I, 374 S., 110 Abb., 23 Tab., New York, London: Academic Press.
- Shastri, A., Singh, P. J., Krishnakumar, S., Das, A. K. & Raja Sekhar, B. N. (2017). *Phys. Chem. Chem. Phys.* **19**, 6454–6469.
- Singh, P. J., Shastri, A., D'Souza, R., Bhaskara Rao, S. V. N. & Jagatap, B. N. (2012). *J. Quant. Spectrosc. Radiat. Transfer*, **113**, 267–278.
- Singh, P. J., Shastri, A., D'Souza, R. & Jagatap, B. N. (2013). *J. Quant. Spectrosc. Radiat. Transfer*, **129**, 204–213.
- Singh, P. J., Shastri, A., Sampath Kumar, R., Jha, S. N., Rao, S. V. N. B., D'Souza, R. & Jagatap, B. N. (2011). *Nucl. Instrum. Methods Phys. Res. A*, **634**, 113–119.
- Sivaraman, B., Nair, B. G., Raja Sekhar, B. N., Jones, N. C., Hoffmann, S. V. & Mason, N. J. (2014). *Chem. Phys. Lett.* **608**, 404–407.
- Śmiełek, M. A., Guthmuller, J., MacDonald, M. A., Zuin, L., Delwiche, J., Hubin-Franskin, M., Lesniewski, T., Mason, N. J. & Limão-Vieira, P. (2017). *J. Quant. Spectrosc. Radiat. Transfer*, **200**, 206–214.
- Sneep, M., Ityaksov, D., Aben, I., Linnartz, H. & Ubachs, W. (2006). *J. Quant. Spectrosc. Radiat. Transfer*, **98**, 405–424.
- Stein, T., Bandyopadhyay, B., Troy, T. P., Fang, Y., Kostko, O., Ahmed, M. & Head-Gordon, M. (2017). *Proc. Natl Acad. Sci.* **114**, E4125–E4133.
- Strählmán, C., Kivimäki, A., Richter, R. & Sankari, R. (2016). *J. Phys. Chem. A*, **120**, 6389–6393.
- Tasumi, M. & Nakata, M. (1985). *J. Mol. Struct.* **126**, 111–124.
- Tiedje, H. F., DeMille, S., MacArthur, L. & Brooks, R. L. (2001). *Can. J. Phys.* **79**, 773–781.
- Viswanathan, K. S., Sankaran, K. & Sundararajan, K. (2006). *Matrix Isolation Spectroscopy in Atmospheric Chemistry*. In *Encyclopedia of Analytical Chemistry*. New York: John Wiley and Sons Ltd.
- Whittle, E., Dows, D. A. & Pimentel, G. C. (1954). *J. Chem. Phys.* **22**, 1943.
- Wilkinson, I., Boguslavskiy, A. E., Mikosch, J., Bertrand, J. B., Wörner, H. J., Villeneuve, D. M., Spanner, M., Patchkovskii, S. & Stolow, A. (2014). *J. Chem. Phys.* **140**, 204301.
- Wu, Y. J., Chen, H., Camacho, C., Witek, H. A., Hsu, S., Lin, M., Chou, S., Ogilvie, J. F. & Cheng, B. (2009). *Astrophys. J.* **701**, 8–11.
- Wu, Y.-J., Lin, M.-Y., Chou, S.-L., Chen, H.-F., Lu, H.-C., Chen, H.-K. & Cheng, B.-M. (2010). *Astrophys. J.* **721**, 856.
- Wu, Y., Wu, C. Y. R., Chou, S., Lin, M., Lu, H., Lo, J. & Cheng, B. (2012). *Astrophys. J.* **746**, 175.
- Young, N. A. (2014). *Coord. Chem. Rev.* **277–278**, 224–274.